Supporting Information for

Unified Fracture Criterion for Brittle 2D Materials

Shenda Jiang[a,#], Israel Greenfeld[b,#], Lin Yang[a,*], Weilong Yin[a], Xiaodong He[a], H. Daniel Wagner [b,*]

[a]*National Key Laboratory of Science and Technology on Advanced Composites in Special Environments, Center for Composite Materials and Structures, Harbin Institute of Technology, Harbin 150080, China*

[b]*Department of Molecular Chemistry and Materials Science, Weizmann Institute of Science, Rehovot 76100, Israel*

[#]These authors contributed equally to this work.

[*]Email: L.Y. Linyang@hit.edu.cn, H.D.W Daniel.Wagner@weizmann.ac.il

S1 Selection and validation of interatomic potentials

S1.1 AIREBO potential for modeling fracture behavior of graphene

The fracture behavior of graphene is described using the Adaptive Intermolecular Reactive Empirical Bond Order (AIREBO) potential. This potential consists of three components: the Lennard-Jones (LJ) potential, the torsional potential, and the Reactive Empirical Bond Order (REBO) potential. The LJ potential accounts for the van der Waals interactions between atoms, while the torsional term captures the energy contribution from single-bond torsion interactions. The REBO term describes the interaction energy between atoms i and j using the following expression:

$$E_{ij}^{REBO} = V_{ij}^{R}(r_{ij}) + b_{ij}V_{ij}^{A}(r_{ij}) \tag{S1}$$

Here, $V_{ij}^{R}(r_{ij})$ represents the repulsive potential, $V_{ij}^{A}(r_{ij})$ denotes the attractive potential, and b_{ij} is the bond order function. The total energy of the system in the AIREBO potential is calculated by summing over these pairwise interactions, and is given by the following expression:

$$E_{AIREBO} = \frac{1}{2}\sum_{i}\sum_{j\neq i}\left[E_{ij}^{REBO} + E_{ij}^{LJ} + \sum_{k\neq i,j}\sum_{l\neq i,j,k}E_{kijl}^{tors}\right] \tag{S2}$$

To avoid unphysical strain hardening in the stress–strain curves, the cutoff distance for C–C bonds in the AIREBO potential was modified to 1.92 Å[1]. This modified AIREBO potential has been widely used in simulations of brittle fracture in monolayer graphene and has been demonstrated to accurately reproduce its mechanical behavior.

S1.2 Tersoff potential for modeling fracture behavior of h-BN

The fracture behavior of h-BN is described using the extended Tersoff potential (BN-EXTeP). Its functional form is expressed as follows:

$$E = \frac{1}{2}\sum_{i,j} f_C\left(r_{ij}\right)\left[V_R\left(r_{ij}\right) - B_{ij}V_A\left(r_{ij}\right)\right] \tag{S3}$$

Here, $V_R\left(\mathrm{r}_{ij}\right)$ and $V_A\left(\mathrm{r}_{ij}\right)$ represent the repulsive and attractive potentials, respectively; B_{ij} is the total bond order function, and $f_c\left(r_{ij}\right)$ is the smooth cutoff function. The expression for $f_c\left(r_{ij}\right)$ is given by:

$$f_C\left(r_{ij}\right) = \begin{cases} 1 & r \le R\text{-}D \\ \frac{1}{2}\left[1 - \sin\left(\frac{\pi\left(r-R\right)}{2D}\right)\right] & \left|R-r\right| < D \\ 0 & r \ge R + D \end{cases} \tag{S4}$$

This potential has been demonstrated to accurately reproduce the mechanical behavior of both pristine and defective h-BN structures. To eliminate the unphysical hardening behavior observed under large deformations, the cutoff function parameters R and D in the BN-EXTeP potential were modified to 1.75 and 0, respectively[2, 3].

S1.3 REBO potential for modeling fracture behavior of MoS_2

The fracture behavior of MoS_2 is described using the Reactive Empirical Bond Order (REBO) potential. Its general functional form is given as:

$$E_b = \frac{1}{2}\sum_{i\neq j} f_{ij}^{C}\left(r_{ij}\right)\left[V^{R}\left(r_{ij}\right) - b_{ij}V^{A}\left(r_{ij}\right)\right] = \frac{1}{2}\sum_{i\neq j} f_{ij}^{C}\left(r_{ij}\right)\left[\left(\left(1+\frac{Q}{r_{ij}}\right)A\cdot e^{-\alpha\cdot r_{ij}} - b_{ij}B\cdot e^{-\beta\cdot r_{ij}}\right)\right] \tag{S5}$$

Here, E_b is the total binding energy of the system, and r_{ij} is the interatomic distance between atoms i and j. $V^{R}\left(\mathrm{r}_{ij}\right)$ and $V^{A}\left(\mathrm{r}_{ij}\right)$ represent the pairwise repulsive and attractive potentials, respectively.

$f_{ij}^{C}\left(r_{ij}\right)$ is the cutoff function, and b_{ij} is the bond order term. In more detailed formulations, parameters such as Q、α and β are primarily related to geometric properties like equilibrium distances, while A and B determine the energy contributions of the attractive and repulsive interactions.

The REBO potential is capable of describing covalent bond breaking, defect evolution, and nonlinear deformation behavior in MoS_2 structures. To eliminate the unphysical strain hardening caused by the switching function in the original REBO potential, the cutoff radii were modified and the repulsive and attractive terms were rescaled by a factor of approximately 0.7. This adjustment ensures that the simulated mechanical strength matches the results obtained from density functional theory (DFT) calculations[4, 5]. The specific parameter adjustments for the cutoff radii of Mo-Mo, Mo-S, and S-S interactions are listed in Table S1.

Table S1. Cutoff Radii for Mo–Mo, Mo–S, and S–S Interactions Before and After Adjustment

REBO	R_{min}/R_{max} (Mo-Mo)	R_{min}/R_{max} (Mo-S)	R_{min}/R_{max} (S-S)
Before Adjustment	3.50/3.80	2.75/3.05	2.30/3.00
After Adjustment	4.50/5.00	2.85/2.85	1.10/2.80

S1.4 ReaxFF potential for modeling fracture behavior of Ti_3C_2

The fracture behavior of Ti_3C_2 is modeled using the Reactive Force Field (ReaxFF). ReaxFF is well-suited for capturing the formation and breaking of covalent bonds in complex systems. The total system energy is expressed as:

$$E_{system} = E_{bond} + E_{over} + E_{under} + E_{val} + E_{pen} + E_{tors} + E_{conj} + E_{vdWaals} + E_{Coulomb} \quad \text{(S6)}$$

Here, E_{bond} is the bond energy term, which depends on the bond order; E_{over} and E_{under} are penalty terms for over-coordination and under-coordination, respectively; E_{val} accounts for energy associated with valence angle deformations; E_{pen} is a penalty term for specific bonding configurations; E_{tors} represents the energy due to torsional strain; E_{conj} considers conjugation effects in π-bond systems; $E_{vdWaals}$ and $E_{Coulomb}$ account for van der Waals and Coulomb interactions, respectively.

S1.5 Validation of interatomic potentials

The interatomic potentials described above have been widely used to investigate both the in-plane and interlayer mechanical properties of the corresponding two-dimensional materials. These potentials are capable of accurately capturing the structural characteristics and fracture behavior of monolayer 2D systems. To validate the applicability of these force fields, particularly their effectiveness in evaluating fracture toughness in the presence of defects, we constructed nearly square, defect-free monolayer nanosheets and examined their stress-strain responses under uniaxial tensile loading. The in-plane dimensions of the simulated crystal structures ranged from 10 nm × 10 nm to 15 nm × 15 nm. Detailed simulation parameters and computational procedures are provided in Section S3.

By comparing the molecular dynamics (MD) simulation results with those from density functional theory (DFT) calculations reported in the literature, we found that the stress–strain curves of graphene, h-BN, and MoS_2 are in good agreement with previous DFT results. For Ti_3C_2,

however, some deviations were observed between the MD-derived stress-strain curves and the corresponding DFT data. Studies have shown that $Ti_3C_2T_x$ exhibits brittle fracture behavior at room temperature, indicating that crack propagation in Ti_3C_2 is primarily governed by its atomic bond strength. To address the discrepancy between MD simulations and the accuracy of the reactive force field, we adopted a maximum critical fracture stress criterion, as suggested by previous studies[6]. Based on the DFT data presented in Figure S3, the maximum critical fracture stresses for Ti_3C_2 are defined as 54 GPa under tensile loading along the zigzag direction and 48 GPa along the armchair direction. For a detailed description of the maximum critical fracture stress criterion, please refer to our previous work[6].

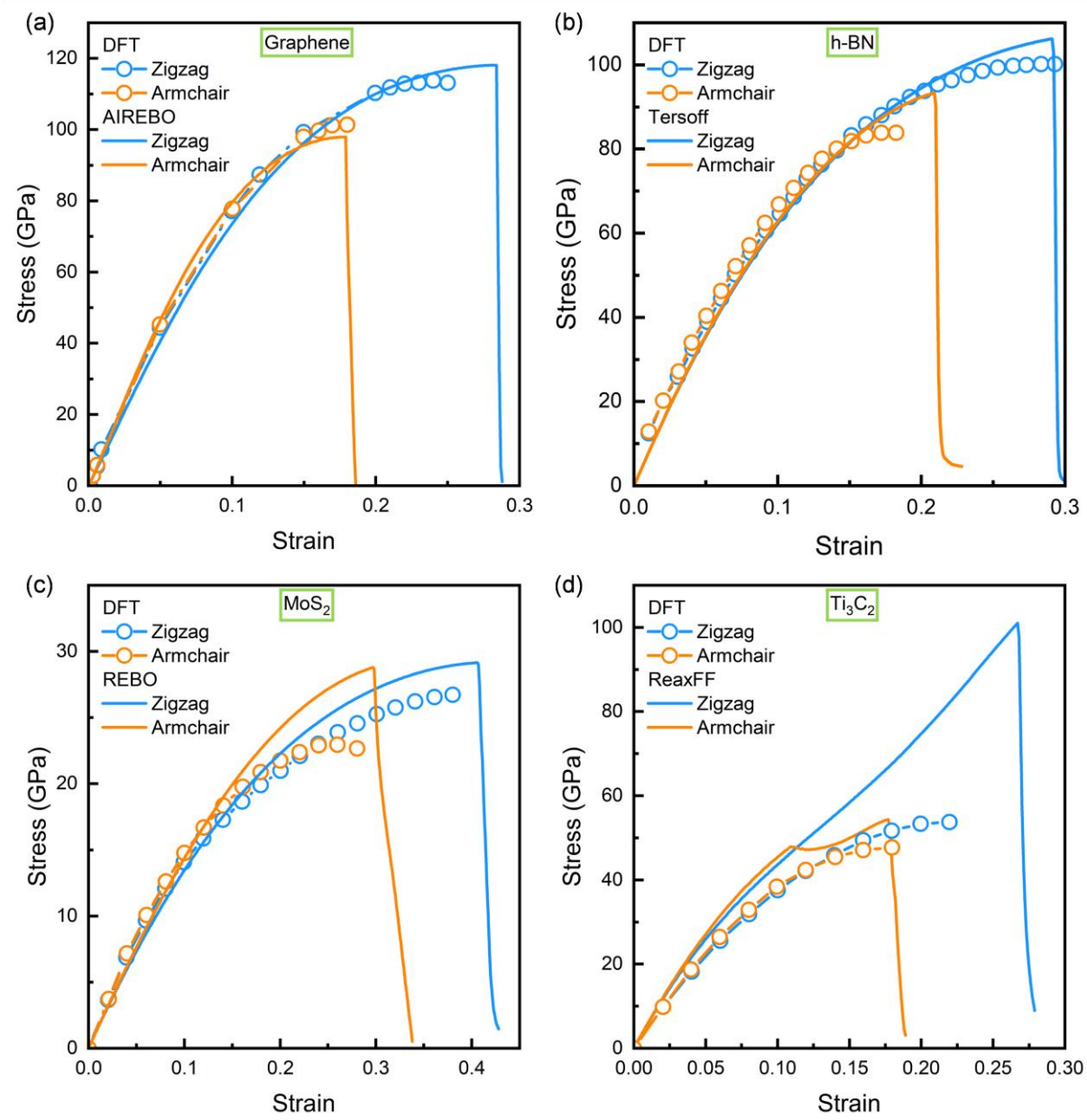

Figure S1. Stress-strain curves of four two-dimensional materials obtained from DFT and MD simulations: (a) graphene, (b) h-BN, (c) MoS_2, and (d) Ti_3C_2. The DFT data are taken from existing literature[4, 7, 8, 9, 10].

S2 Simulation details of fracture in two-dimensional materials

Prior to uniaxial tensile loading, quasi-static relaxation of the monolayer nanosheets was

performed using the conjugate gradient method to obtain locally minimized energy configurations. The energy and force convergence tolerances were set to 1×10^{-10} kcal/mol and 1×10^{-10} (kcal/mol)/Å, respectively. The monolayer 2D structures were then fully relaxed for 50 ps under the NPT ensemble (constant number of atoms, pressure, and temperature) to release residual internal stresses and achieve stable configurations. Tensile loading was applied under the NPT ensemble by gradually adjusting the size of the simulation box along the loading direction, with a constant engineering strain rate of 10^9/s. The simulations were conducted at a quasi-static temperature of 1 K to minimize the influence of thermal fluctuations on the atomistic fracture behavior of brittle materials. The time step for tensile loading was set to 0.2 fs, and the loading direction was perpendicular to the orientation of the pre-existing crack.

The in-plane stress was calculated using the virial theorem, with the monolayer thickness of graphene, h-BN, MoS_2, and Ti_3C_2 taken as 3.4 Å, 3.35 Å, 6.5 Å, and 4.64 Å, respectively[2, 5, 11]. Far-field stress was obtained by averaging the tensile stress over all atoms within a rectangular region located away from the central crack. Periodic boundary conditions were applied in all three directions (X, Y, and Z). A vacuum layer of 40 Å was introduced along the Z direction to provide sufficient space for tensile deformation and to eliminate interlayer interactions. All simulation results were visualized and analyzed using the OVITO software[12].

S3 Analytical expression of crack length and center pre-existing crack

S3.1 Mathematical expression of crack length

By analyzing the repeating unit cell and crack dimensions defined in Figure 3, the expression

for the crack length can be obtained as follows:

$$\begin{cases} 2a_{ZZ} = \dfrac{\sqrt{3}}{2}\left(N_v + \left\lceil \dfrac{N_v}{N_v+1} \right\rceil \right) r^0 \\ 2a_{AC} = \dfrac{3}{2} N_v r^0 \end{cases} \quad \text{Graphene and h-BN} \tag{S7}$$

$$\begin{cases} 2a_{ZZ} = \dfrac{\sqrt{3}}{2}\left(N_v + \left\lceil \dfrac{N_v}{N_v+1} \right\rceil - \left\lfloor \dfrac{N_v}{3} \right\rfloor \right) r^{0\prime} \\ 2a_{AC} = \begin{cases} N_v r^{0\prime}, & \mathrm{mod}\left(N_v/3\right) = 0 \\ \left(N_v + \dfrac{1}{2} \right) r^{0\prime}, & \mathrm{mod}\left(N_v/3\right) \neq 0 \end{cases} \end{cases} \quad \mathrm{MoS_2} \tag{S8}$$

$$\begin{cases} 2a_{ZZ} = \dfrac{\sqrt{3}}{2} m\left(N_v\right) r^{0i\prime} \\ 2a_{AC} = \begin{cases} \dfrac{3m\left(N_v\right)}{4} r^{0i\prime} & \mathrm{mod}\left(\dfrac{m\left(N_v\right)-2}{4} \right) = 0 \\ \left(m\left(N_v\right) - \left\lfloor \dfrac{m\left(N_v\right)+1}{4} \right\rfloor \right) r^{0i\prime} & \text{otherwise} \end{cases} \end{cases} \quad \mathrm{Ti_3C_2} \tag{S9}$$

Here N_v is the number of atoms removed to create the defect, r^0 is the covalent bond length in graphene and h-BN, $r^{0\prime}$ is the projected bond length of the Mo–S bond in the two-dimensional plane, $r^{0i\prime}$ is the projected bond length of the Ti–C bond in the two-dimensional plane (the bond lengths are defined in Figure 3), and $m\left(N_v\right)$ is the number of discrete advancement steps of crack growth (specified in Table S2 ahead).

S3.2 Pre-existing central crack structures of h-BN and MoS_2

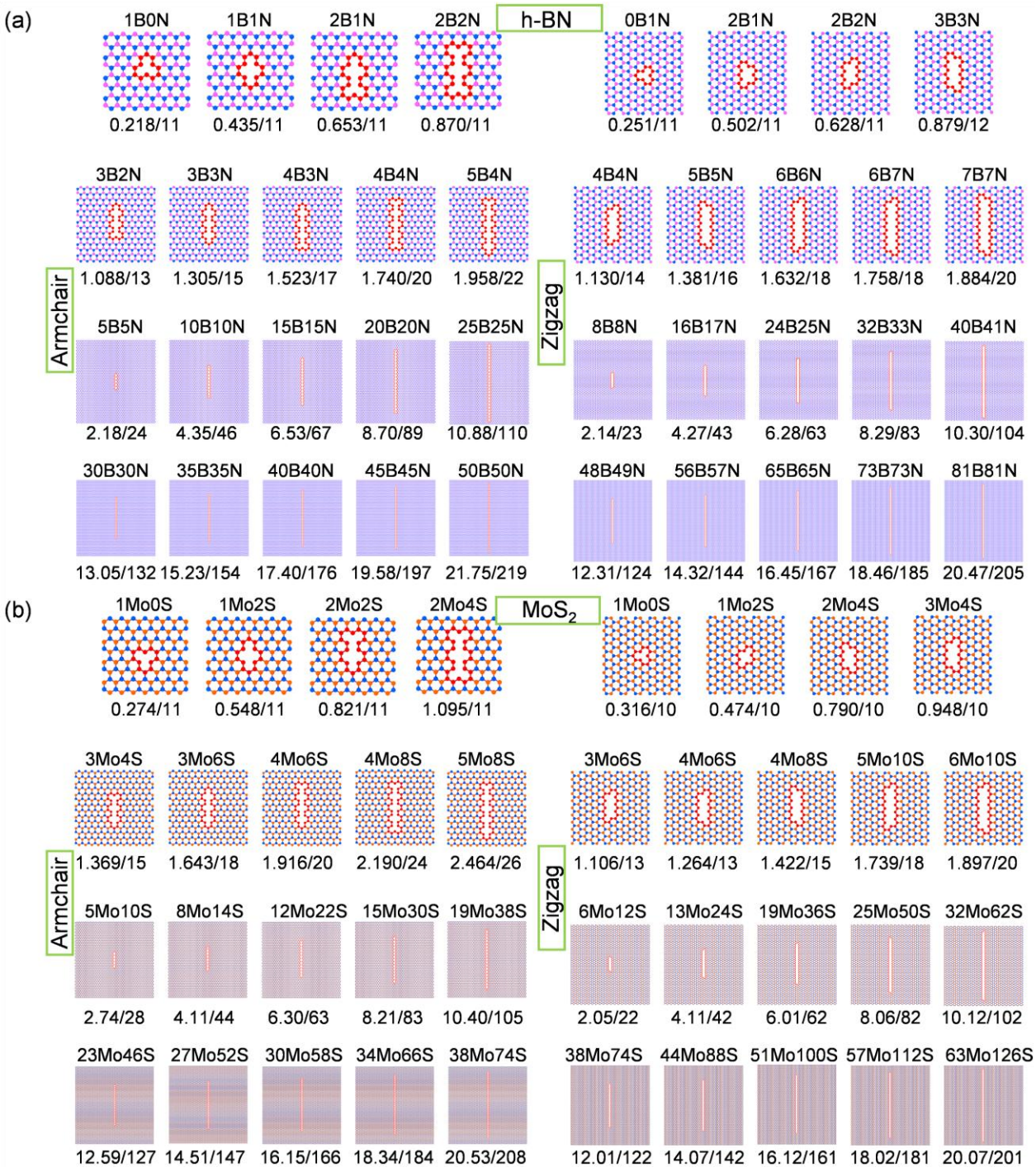

Figure S2. Central pre-cracked structures. (a) h-BN and (b) MoS_2. The number and type of removed atoms is indicated above each configuration, and the corresponding crack-to-width ratio ($2a/2w$) is labeled below.

S3.3 Atomic removal sequence in defective 2DMs

For graphene, slit crack is constructed by sequentially removing carbon atoms along the central axis of the structure, with the crack propagating along either the armchair (AC) or zigzag (ZZ) direction. In the case of h-BN, the crack is formed by alternately removing boron (B) and nitrogen (N) atoms along the central axis, resulting in a nearly symmetric linear crack. For MoS_2, slit crack is generated by alternately removing a molybdenum (Mo) atom and its two bonded sulfur (S) atoms located above and below the central axis. Specifically, to create a through-thickness crack, one first removes an Mo atom, followed by the removal of the two S atoms bonded above and below it. This sequence is then repeated to progressively extend the crack.

For Ti_3C_2, the slit crack is constructed by sequentially removing atoms from its five-layer structure composed of Ti, C, Ti, C, and Ti layers, following a specific four-step cycle. First, a Ti atom is removed from the middle (third) layer. In the second step, a C atom and a Ti atom are removed: for the AC model, these atoms are taken from the second and fifth layers, while for the ZZ model, they are from the fourth and first layers. In the third step, another pair of atoms is removed: in the AC model, this involves removing a Ti atom from the first layer and a C atom from the fourth layer, whereas in the ZZ model, it involves removing a C atom from the second layer and a Ti atom from the fifth layer. The fourth step repeats the second, removing the C and Ti atoms from the same layers as before. By cyclically repeating this removal pattern, a straight and through-thickness crack of arbitrary length can be formed.

S4 Theoretical Model for Fracture of 2D Materials - details

S4.1 Nonlinear elasticity

The monolayers elastic behavior is nonlinear, likely a result of prestresses embedded in the atomic structure, significantly affecting fracture toughness. Nonlinearity is commonly expressed by the empirical Ramberg-Osgood equation[13, 14], $\frac{\varepsilon}{\varepsilon_0}=\frac{\sigma}{\sigma_0}+\alpha\left(\frac{\sigma}{\sigma_0}\right)^n$, where σ is the far-field (applied) stress, ε_0 and σ_0 are reference strain and stress, α is a dimensionless constant, and n is a strain hardening/softening exponent. Substituting $\varepsilon_0=\sigma_0/E$, where E is the modulus (slope at the origin of the stress-strain curve), and rewriting[6]:

$$\varepsilon=\frac{\sigma}{E}\left[1+\alpha\left(\frac{\sigma}{\sigma_0}\right)^{n-1}\right] \tag{S10}$$

The first term specifies the linear part of the elasticity, whereas the second term describes the nonlinear part. This equation has four independent parameters, E, α, σ_0 and n, which should be reduced to avoid over-parametrization when fitting to stress-strain data. In materials with plastic behavior, σ_0 is typically set as the yield strength; however, the atomic monolayers in this study do not yield and maintain their elasticity until brittle fracture. We therefore leave σ_0 as a free parameter, and prefer to set $\alpha=1$. Note that the exponent n, which in ductile materials reflects plastic strain hardening/softening, here, instead, determines the degree of nonlinearity.

S4.2 Nonlinear energy release rate

Fracture mechanics uses energy balance as a criterion for fracture, instead of a maximum allowed stress or the material strength. Some of the elastic energy stored in a structure under load

is released when a crack propagates, providing the necessary energy needed to break bonds across the crack faces. Prior to the presence of a crack, the stored elastic energy may be obtained by integrating the stress-strain curve over the volume around the crack from where it is released. In the following analysis, the J integral method is used, which applies to nonlinear elasticity. J is the strain energy release rate, that is, the amount of energy released per unit area of an incremental increase in crack surface. We use the EPRI engineering approach for elastic-plastic fracture analysis[14, 15], and apply it to a center-cracked plate of finite width in tension[6]. Similar solutions are available in[14, 15] for other structures and loading configurations. The nonlinear elasticity is described by the empirical Ramberg-Osgood Equation (S10).

For the linear elastic part, $J_l = G$, where G is the cohesive fracture energy per unit crack area, and the energy release rate is given by the Griffith model[6, 14, 16]:

$$J_l = \frac{\pi h \sigma^2 a}{E} \tag{S11}$$

where a is the crack half-length. The parameter h is a dimensionless geometry correction factor, which depends on the ratio a/w, where w is the monolayer half-width ($h = 1$ when $a \ll w$)[17].

For the nonlinear elastic part, the energy release rate is given by[6, 14, 15]:

$$J_{nl} = \frac{\alpha \sigma_0^2 a}{E}\left(1-\frac{a}{w}\right)^{-n} h_1 \left(\frac{\sigma}{\sigma_0}\right)^{n+1} \tag{S12}$$

Plane stress applies as the monolayers are very thin plates. The dimensionless geometry correction factor h_1 is tabulated in[14, 15], depending on the ratio a/w and the exponent n.

The total J is obtained by adding the linear and nonlinear parts and rearranging[6, 14, 15]:

$$J = J_l + J_{nl} = \frac{\pi\sigma^2 a}{E}\left[h + \frac{\alpha}{\pi}h_1\left(1-\frac{a}{w}\right)^{-n}\left(\frac{\sigma}{\sigma_0}\right)^{n-1}\right] \quad \text{(S13)}$$

For the present study, this equation is simplified by substituting $\alpha = 1$ and using large plates ($a \ll w$)[6]:

$$J = \frac{\pi\sigma^2 a}{E}\left[1 + \frac{h_1}{\pi}\left(\frac{\sigma}{\sigma_0}\right)^{n-1}\right] \quad \text{(S14)}$$

where h_1 may be obtained by extrapolating the tabular data in[14, 15] for $a/w = 0$. However, the tabulated h_1 is not applicable because it was calculated for continuum solids rather than for discrete materials, and therefore fitting must be used.

Equation (S14) may instead be derived as follows[6]. The elastic energy density in a defect-free monolayer is obtained by integrating Equation (S10), $\int_0^{\varepsilon}\sigma d\varepsilon = \sigma\varepsilon - \int_0^{\sigma}\varepsilon d\sigma$. In the presence of a crack in a linear-elastic, infinite-width plate, the elastic energy is released from a volume $2\pi a^2 B$, where B is the plate thickness. Thus, the energy released by a crack $2a$ is $U_e = \frac{\pi\sigma^2 a^2 B}{E}\left[1 + \frac{2nk}{n+1}\left(\frac{\sigma}{\sigma_0}\right)^{n-1}\right]$, where the dimensionless factor k is added to adjust the release volume for nonlinearity ($\alpha = 1$). The energy release rate with respect to an incremental growth in crack area $dA = 2Bda$, is given by $J = dU_e/dA$. Hence, $J = \frac{\pi\sigma^2 a}{E}\left[1 + \frac{2nk}{n+1}\left(\frac{\sigma}{\sigma_0}\right)^{n-1}\right]$, which is the same as Equation (S14) when the term $\frac{2nk}{n+1}$ is replaced by $\frac{h_1}{\pi}$.

S4.3 Quantized energy release rate

The atomic-scale monolayers investigated in this study cannot be considered continuum solids, as their structure is discrete. To address the discreteness, the theory of quantized fracture mechanics

(QFM) developed by Pugno and Ruoff[18] is applied. QFM assumes quantization of the fracture toughness, attributed to the discrete propagation of a crack in an atomic-scale structure. In other words, the crack propagates by elimination of atoms one-by-one, creating atom vacancies along the propagation path. Consequently, the energy release rate is discrete, increasing or decreasing in steps that correspond to the discrete steps in crack length. Thus, in an atomic-scale structure the length of a crack is a discrete function of the number of vacancy atoms. To recover continuity, the energy release rate (Equation (S14)) is averaged along the crack path over a distance of atomic scale, q, termed the fracture quantum:

$$J = \frac{1}{q}\int_{a}^{a+q} J(a)\, da = \frac{\pi\sigma^2 (a + q/2)}{E}\left[1 + \frac{h_1}{\pi}\left(\frac{\sigma}{\sigma_0}\right)^{n\text{-}1}\right] \tag{S15}$$

Note that when the ratio a/w is not negligible, the averaging of J requires integration of Equation (S13).

The fracture quantum q can be estimated based on the incremental crack length corresponding to each minimal discrete step of crack propagation, which is typically associated with the geometric change caused by the removal of one or a specific group of atoms[6, 18]:

$$q \cong \frac{2a}{m(N_v)} \tag{S16}$$

Here, $m(N_v)$ denotes the number of discrete advancement steps of crack growth induced by progressively breaking bonds and/or removing atoms. The denominator of Equation (S16) is a function of the number of missing atoms (N_v), rather than just N_v as suggested in the references cited above; the reason for this is that, in the complex structures studied here, the crack growth

steps depend on the specific atoms removal sequence. For example, in some cases a removed atom does not cause a growth step along the crack but a lateral step which does not extend the crack, or a removed atom overlaps an atom in another layer above or below it.

The value of the fracture quantum q is obtained by taking the limit in Equation (S16), specifically $q = \lim_{N_v \to \infty} 2a / m(N_v)$. The associated parameters and computed results are summarized in Table S2. Definitions of crack length are based on Equations (S7)–(S9), the atomic removal sequence is described in Section S3.3, and the values of bond lengths and their projections are presented in Figure 3. Due to the hexagonal symmetry of graphene, h-BN, and MoS_2, the fracture quanta along the AC and ZZ directions are of the same order of magnitude. Accordingly, the number of discrete advancement steps of crack growth for the AC-oriented cracks in these three materials is given by: $2N_v$, $2N_v$, and $2\lceil 2N_v/3 \rceil$, respectively, which is twice the number for the corresponding ZZ-oriented cracks. For Ti_3C_2, both the defect length and fracture quantum definitions are based on our previous work[6], owing to its quasi-hexagonal lattice structure.

A distinct pattern emerges from the results presented in Table S2: the limit values of the function in Equation (S16) are consistently $q_{AC} \cong \frac{3}{4} r$ for all armchair cases and $q_{ZZ} \cong \frac{\sqrt{3}}{2} r$ for all zigzag cases, where r is the projection of the bond length on the 2DM plane.

Table S2. Summary of the parameters and results used in the calculation of fracture quantum.

2DMs	Defect Type	$m(N_v)$	Limit result	r^0 or $r^{0'}$ or $r^{0i'}$ (Å)	q (Å)
Graphene	AC	$2N_v$	$\frac{3}{4}r^0$	1.42	1.07
	ZZ	N_v	$\frac{\sqrt{3}}{2}r^0$		1.23
h-BN	AC	$2N_v$	$\frac{3}{4}r^0$	1.45	1.09
	ZZ	N_v	$\frac{\sqrt{3}}{2}r^0$		1.26
MoS_2	AC	$2\lceil 2N_v/3 \rceil$	$\frac{3}{4}r^{0'}$	1.825	1.37
	ZZ	$\lceil 2N_v/3 \rceil$	$\frac{\sqrt{3}}{2}r^{0'}$		1.58
Ti_3C_2	AC	$\left\lfloor \frac{4N_v+3}{7} \right\rfloor$	$\frac{3}{4}r^{0i'}$	1.77	1.33
	ZZ	$\left\lfloor \frac{4N_v+3}{7} \right\rfloor$	$\frac{\sqrt{3}}{2}r^{0i'}$		1.53

The fracture quantum is a physical quantity closely tied to the discrete atomic structure of 2DMs and plays a crucial role in characterizing each specific nanomaterial. In future research, we will aim to estimate the q-value of different materials more accurately and universally, based on its physical essence as the minimum discrete increment of crack propagation.

S4.4 Fracture toughness and critical defect

J in Equation (S15) is the crack driving force, which depends on the applied stress and the defect length. For very long defects, where $a \gg q/2$ and $\sigma \ll \sigma_0$, this equation converges to $J \cong \pi\sigma^2 a / E$, the classic Griffith expression for linear elasticity, resembling the fracture toughness

of a continuum solid. However, for short defects, the effect of the quantization and nonlinearity becomes significant. The material resistance, J_R, is given by setting $\sigma = \sigma_f$, the far-field stress at fracture for a given defect a:

$$J_R = \frac{\pi\sigma_f^2\left(a + q/2\right)}{E}\left[1 + \frac{h_1}{\pi}\left(\frac{\sigma_f}{\sigma_0}\right)^{n-1}\right] \tag{S17}$$

For crack growth to be stable, the rate of change of the driving force with respect to crack length should be lower than or equal to that of the resistance, that is, $\frac{\partial J}{\partial a} \le \frac{\partial J_R}{\partial a}$ [6, 14].

The critical defect half-length, a, may be obtained by rewriting Equation (S17) with the critical energy release rate J_{Ic}, the energy that corresponds to very long defects (the asymptotic value of J_R). In brittle materials such as the studied 2DMs, J_R is fairly constant [14], and therefore J_{Ic} can be used for all defect lengths. Thus

$$a = \frac{EJ_{Ic}}{\pi\sigma_f^2\left[1 + \frac{h_1}{\pi}\left(\frac{\sigma_f}{\sigma_0}\right)^{n-1}\right]} - \frac{q}{2} \tag{S18}$$

where the fracture toughness is specified by $K_{Ic} = \sqrt{EJ_{Ic}}$. This equation states the unified fracture criterion proposed in this study for atomic monolayers. The equation is used for fitting the molecular dynamic simulation fracture results of the monolayers investigated in the study. In this equation, for each monolayer type, E, σ_0 and n are obtained by fitting Equation (S10) to the stress-strain simulation of the defect-free monolayer; q is estimated by Equation (S16); a and σ_f are data pairs at fracture obtained by the simulation of defected monolayers with varying defect lengths; and h_1 and J_{Ic} (or K_{Ic}) are used as fitting parameters. The parameter h_1 can alternatively be obtained from the tables in [14, 15]; however, its use as fitting parameter allows generalization and

better accuracy of the solution.

S4.5 Pristine strength

The pristine, defect-free strength, σ_f^*, may be predicted by solving Equation (S18) (numerically) for $a=0$:

$$\sigma_f^{*2}\left[1+\frac{h_1}{\pi}\left(\frac{\sigma_f^*}{\sigma_0}\right)^{n-1}\right]=\frac{2EJ_{Ic}}{\pi q} \tag{S19}$$

Unlike linear elastic fracture mechanics, the strength prediction does not diverge when there is no defect, because of the finite size of the fracture quantum in atomic-scale structures. According to this relation, in monolayers with a smaller atomic distance (smaller q), the defect-free strength will be higher. Also, as the ratio σ_f^*/σ_0 is typically smaller than unity, when the nonlinearity is more pronounced (small n and small σ_0), the defect-free strength will be smaller as well.

S4.6 Approximate solution

Equations (S18) and (S19) can only be solved numerically for the stress. The following approximation provides an explicit solution for the stress, and offers some interesting insights on the way elastic nonlinearity affects toughness. For that purpose, Equation (S18) is approximated by series expansion of the term in brackets:

$$a+\frac{q}{2}\cong\frac{EJ_{Ic}\left[1-\frac{h_1}{\pi}\left(\frac{\sigma_f}{\sigma_0}\right)^{n-1}\right]}{\pi\sigma_f^2}\cong\frac{EJ_{Ic}}{\pi\sigma_f^2}-\frac{h_1EJ_{Ic}}{\pi^2\sigma_0^2}\left(\frac{\sigma_f}{\sigma_0}\right)^{n-3} \tag{S20}$$

This approximation has accuracy of order $O\left(\left(\sigma_f/\sigma_0\right)^{2(n-1)}\right)$, equivalent to the next term in the expansion, and is satisfactory because, except for very small defects, $\sigma_f \ll \sigma_0$. We define the nonlinearity factor:

$$p = \frac{h_1 E J_{Ic}}{\pi^2 \sigma_0^2} = \frac{2nk}{n+1} \frac{E J_{Ic}}{\pi \sigma_0^2} \tag{S21}$$

where $\frac{2nk}{n+1}$ replaced $\frac{h_1}{\pi}$, as noted at the end of Section S4.2, to reflect the effect of the nonlinearity exponent. k is a dimensionless fitting parameter. The nonlinearity parameter p is of length dimension. The rightmost term in Equation (S20), $p\left(\frac{\sigma_f}{\sigma_0}\right)^{n-3}$, is still dependent on the fracture stress. However, for long defects ($\sigma_f \ll \sigma_0$) it may be neglected, while for short defects ($\sigma_f \to \sigma_0$) it tends to p. Therefore, we approximate the nonlinear term by p, keeping in mind that for long defects it is negligible with respect to a. To compensate for the inaccuracy introduced by this approximation, the parameter k is allowed to be tuned for best fit of the data.

Rearranging, we obtain an explicit expression for the fracture stress:

$$\sigma_f \cong \sqrt{\frac{E J_{Ic}}{\pi\left(a + \frac{q}{2} + p\right)}} \tag{S22}$$

where $\sqrt{E J_{IC}} = K_{IC}$. The pristine, defect-free strength, σ_f^*, may be explicitly expressed by substituting $a = 0$:

$$\sigma_f^* \cong \sqrt{\frac{E J_{Ic}}{\pi\left(\frac{q}{2} + p\right)}} \tag{S23}$$

S4.7 Model validation

The UFM model is purely analytical, derived from the established theories of nonlinear fracture mechanics (NLFM) and quantized fracture mechanics (QFM). Indeed, NLFM uses the empirical Ramberg Osgood (RO) model of elastic-plastic nonlinearity, but this is a commonly

accepted approach in NLFM (see details in Sections S4.1 and S4.2). The UFM parameters (h_1 or p, depending on the model) may be assessed by analytical predictions or by fitting to simulations. The dataset used for validating RO is primarily derived from the MD elastic simulation, whereas the dataset for validating UFM is derived from the MD crack simulation. Thus, these two datasets are created by separate simulations, but are derived using the same MD program and force fields. To alleviate a possible concern regarding the use of similarly derived datasets for validating the UFM model, we backed the RO MD dataset by DFT analysis reported in the literature (see Section S1.5). Furthermore, the UFM fracture toughness results compare reasonably well with theoretical and experimental values reported in the literature for 2DMs (see Section 3.4). The theoretical UFM model fits the simulation results very well, demonstrating that the NLFM theory, originally developed for continuum solids, may be extended for 2DMs by combining with QFM.

S5 Parameter fitting of nonlinear elasticity in 2DMs

To avoid the influence of nonlinear instabilities near the fracture point on the fitting results, 80% of the fracture strain was selected as the cutoff strain. The fitting parameters for Ti_3C_2 were adopted from existing literature studies [10], while those for Ti_2C were taken from Ref. [19]. Fracture mechanics parameters obtained by fitting to the Ramberg–Osgood (RO) equation are summarized in Table 1.

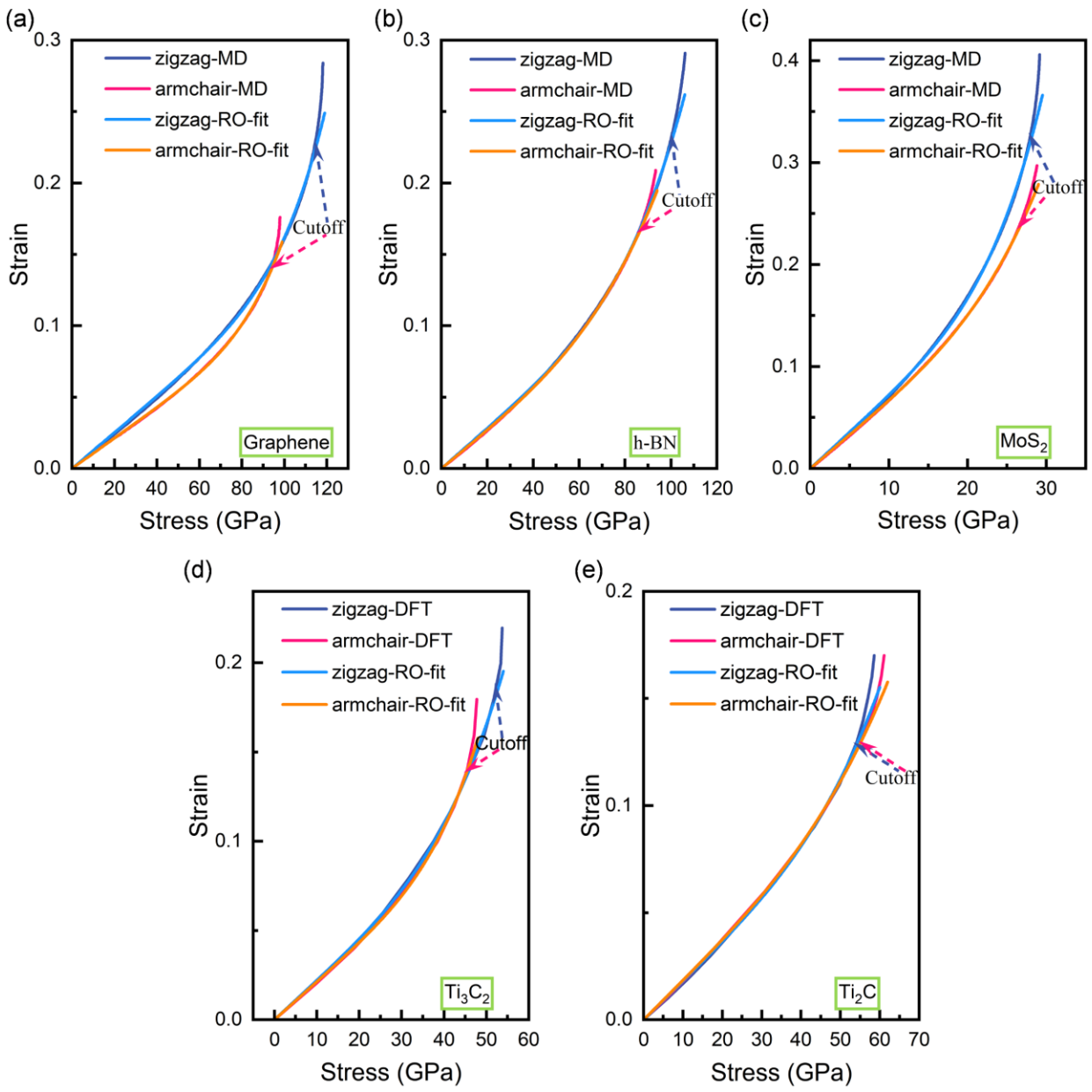

Figure S3. Ramberg–Osgood equation fitting results for four 2D materials: (a) graphene, (b) h-BN, (c) MoS_2, (d) Ti_3C_2, and (e) Ti_2C. The DFT data for Ti_3C_2 and Ti_2C are adopted from existing studies[10, 19].

S6 UFM Model Predictions for Ti_2C

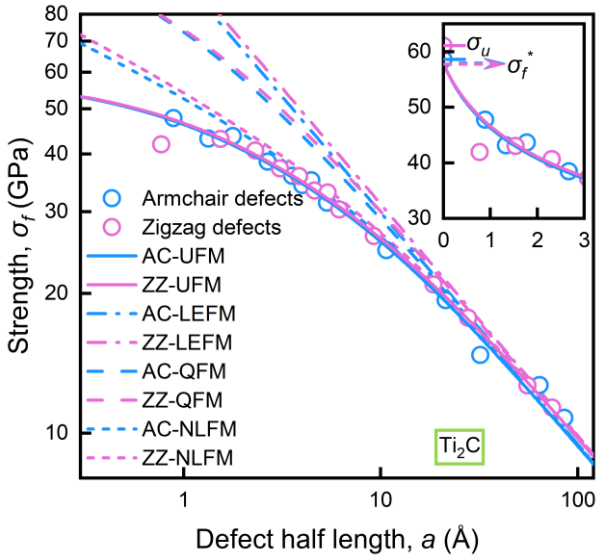

Figure S4. Simulated fracture strength and modeling for Ti_2C. Log–log plot of the fracture strength σ_f versus defect half-length a for Ti_2C with armchair and zigzag defects. Theoretical trendlines based on the unified fracture model (UFM, Equation (S18)) are fitted to the simulation results. For comparison, predictions from LEFM, QFM, and NLFM models are also shown. Inset: linear–linear plot highlighting the predicted pristine strength σ_f^*.

S7. Prediction results of the approximate UFM model

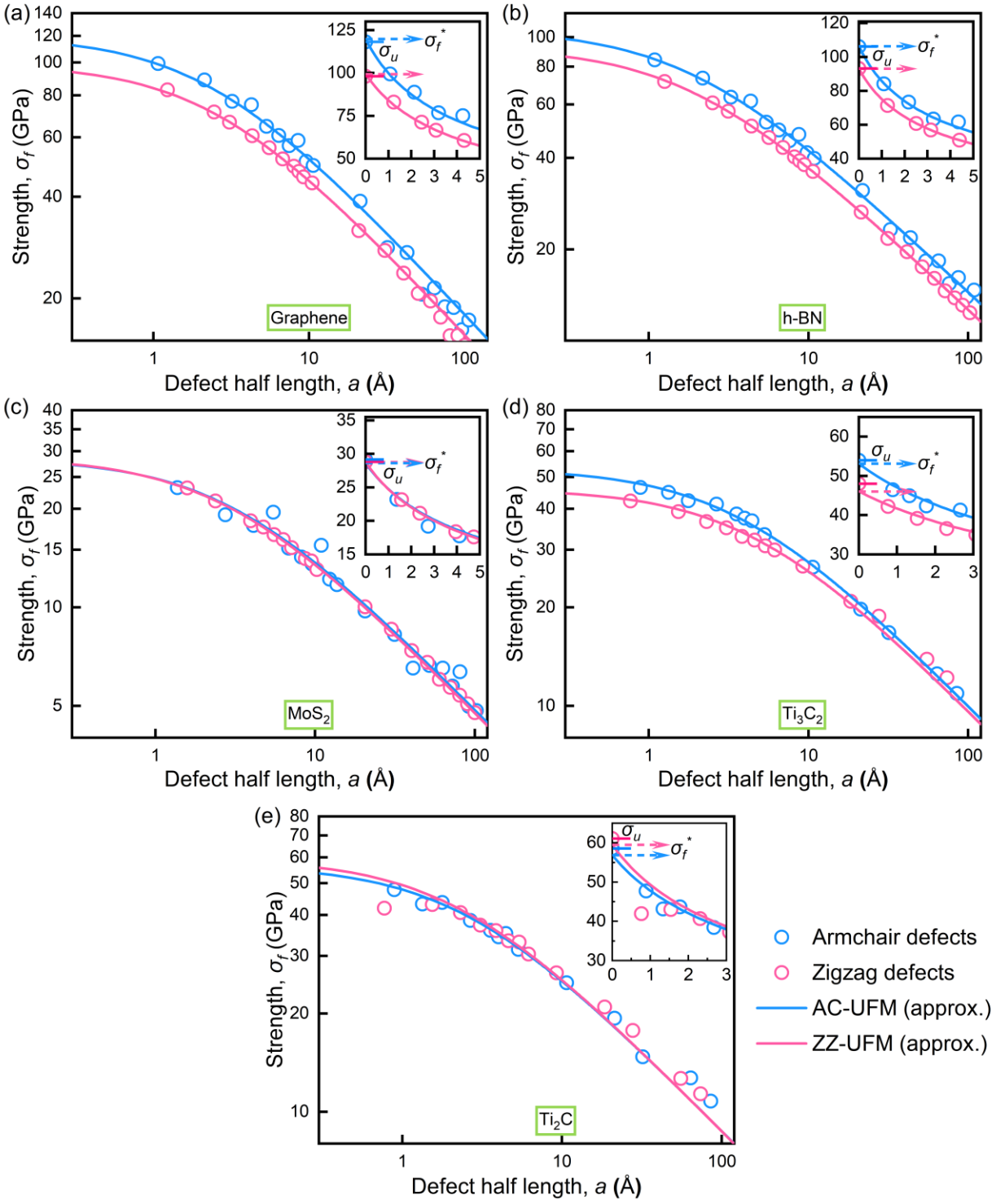

Figure S5. Theoretical trendlines predicted by the approximate UFM model. Log–log plots of the strength of armchair and zigzag defected models ((a) graphene, (b) h-BN, (c) MoS_2, (d) Ti_3C_2, and (e) Ti_2C) versus the defect half-length a. Theoretical trendlines of the approximate unified fracture model (approximate UFM,

Equation (S22)) are fitted to the simulation data.

S8 Driving force/R curves for the fracture behavior of Ti_2C

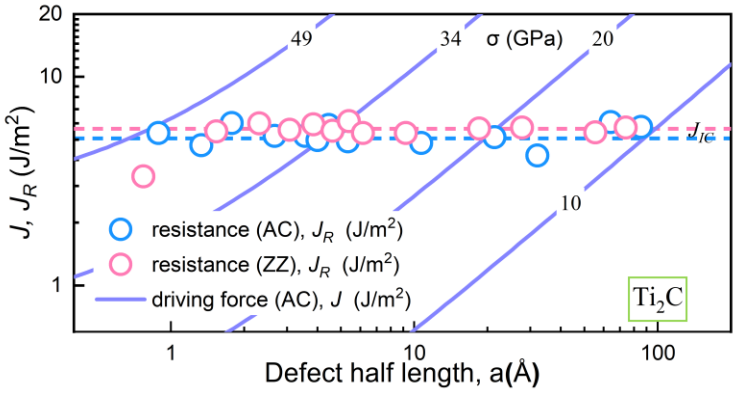

Figure S6. Crack Instability Analysis of Ti_2C. The simulation data are taken from previous work[6], and the definitions of specific parameters are detailed in Figure 10.

References

1. Yin H, Qi HJ, Fan F, Zhu T, Wang B, Wei Y. Griffith criterion for brittle fracture in graphene. *Nano Lett* **15**, 1918-1924 (2015).
2. Zhang G, Chen Y, Yue S, Zhang Y-W, Qin H, Liu Y. A unified strength criterion for two-dimensional materials via bond failure analysis. *J Mech Phys Solids* **181**, 105466 (2023).
3. Chen Y, Qin H, Song J, Liu Z, Liu Y, Pei Q-X. Exploring the structure-property relationship of three-dimensional hexagonal boron nitride aerogels with gyroid surfaces. *Nanoscale* **12**, 10180-10188 (2020).
4. Wang S, *et al.* Atomically sharp crack tips in monolayer MoS_2 and their enhanced toughness

by vacancy defects. *ACS nano* **10**, 9831-9839 (2016).

5. Wu JY*, et al.* Grain-Size-Controlled Mechanical Properties of Polycrystalline Monolayer MoS_2. *Nano Lett* **18**, 1543-1552 (2018).
6. Greenfeld I, Jiang SD, Yang L, Wagner HD. Nonlinear elasticity degrades monolayer fracture toughness. *Acta Materialia* **286**, (2025).
7. Shimada T, Huang K, Lich LV, Ozaki N, Jang B, Kitamura T. Beyond conventional nonlinear fracture mechanics in graphene nanoribbons. *Nanoscale* **12**, 18363-18370 (2020).
8. Yang Y*, et al.* Intrinsic toughening and stable crack propagation in hexagonal boron nitride. *Nature* **594**, 57-61 (2021).
9. Xiong S, Cao GX. Molecular dynamics simulations of mechanical properties of monolayer MoS_2. *Nanotechnology* **26**, (2015).
10. Tian S, Zhou K, Huang C-Q, Qian C, Gao Z, Liu Y. Investigation and understanding of the mechanical properties of MXene by high-throughput computations and interpretable machine learning. *Extreme Mechanics Letters* **57**, (2022).
11. Zhang N, Hong Y, Yazdanparast S, Zaeem MA. Superior structural, elastic and electronic properties of 2D titanium nitride MXenes over carbide MXenes: a comprehensive first principles study. *2D Materials* **5**, 045004 (2018).
12. Stukowski A. Visualization and analysis of atomistic simulation data with OVITO–the Open Visualization Tool. *Modell Simul Mater Sci Eng* **18**, 015012 (2009).
13. Ramberg W, William R s. Description of stress-strain curves by three parameters.). National

Advisory Committee for Aeronatics (1943).

14. Anderson TL. *Fracture Mechanics Fundamentals and Applications*, 4 edn. CRC Press (2017).

15. Kumar V, German MD, Shih CF. An engineering approach for elastic-plastic fracture analysis. In: *EPRI Project*). General Electric Company (1981).

16. Griffith AA. Phenomena of Rupture and Flow in Solids. *Philos Tr R Soc S-A* **221**, 163-198 (1921).

17. Rooke DP, Cartwright DJ. *Compendium of stress intensity factors*. HMSO Ministry of Defence, Procurement Executive (1976).

18. Pugno NM, Ruoff RS. Quantized fracture mechanics. *Philos Mag* **84**, 2829-2845 (2004).

19. Guo Z, Zhou J, Si C, Sun Z. Flexible two-dimensional $Ti_{n+1}C_n$ (n= 1, 2 and 3) and their functionalized MXenes predicted by density functional theories. *Physical Chemistry Chemical Physics* **17**, 15348-15354 (2015).